Naval Research Laboratory

Washington, DC 20375-5320

NRL/MR/5651--16-9700

Reduction of Photodiode Nonlinearities by Adaptive Biasing

Meredith N. Hutchinson
Nicholas J. Frigo

Photonics Technology Branch
Optical Sciences Division

Caitlin R.S. Williams

Hastings College
Hastings, Nebraska

October 14, 2016

REPORT DOCUMENTATION PAGE

Form Approved
OMB No. 0704-0188

1. REPORT DATE *(DD-MM-YYYY)*	**2. REPORT TYPE**	**3. DATES COVERED** *(From - To)*
14-10-2016	Memorandum	21 October 2015 – 15 June 2016

4. TITLE AND SUBTITLE

Reduction of Photodiode Nonlinearities by Adaptive Biasing

5a. CONTRACT NUMBER

5b. GRANT NUMBER

5c. PROGRAM ELEMENT NUMBER

6. AUTHOR(S)

Meredith N. Hutchinson, Nicholas J. Frigo, and Caitlin R. S. Williams*

5d. PROJECT NUMBER

5e. TASK NUMBER

5f. WORK UNIT NUMBER
4973

7. PERFORMING ORGANIZATION NAME(S) AND ADDRESS(ES)

Naval Research Laboratory
4555 Overlook Avenue, SW
Washington, DC 20375-5320

8. PERFORMING ORGANIZATION REPORT NUMBER

NRL/MR/5651--16-9700

9. SPONSORING / MONITORING AGENCY NAME(S) AND ADDRESS(ES)

Office of Naval Research
One Liberty Center
875 North Randolph Street, Suite 1425
Arlington, VA 22203-1995

10. SPONSOR / MONITOR'S ACRONYM(S)

ONR

11. SPONSOR / MONITOR'S REPORT NUMBER(S)

12. DISTRIBUTION / AVAILABILITY STATEMENT

Approved for public release; distribution is unlimited.

13. SUPPLEMENTARY NOTES

*Hastings College, Physics Department, 710 Turner Ave, Hastings, NE 68901

14. ABSTRACT

RF photonic links impress information on modulated optical carriers as a method of transporting high frequency and microwave information over sizeable distances. If the system bandwidth is greater than one octave, the system must contend with the possibility of second order intermodulation distortion (IMD2) creating spurious tones due to nonlinearities. These spurious tones masquerade as signals and impair the performance of the photonic link. Earlier research has shown the utility of defining a nonlinear coefficient that relates the nonlinear second order distortion from two optical tones to the product of the powers of those tones. This nonlinear coefficient was shown to be a function of (i) the bias voltage applied to the photodiode/load resistor combination (Vtot), (ii) the DC level of current through the photodiode, IDC, and (iii) the IMD output frequency.

15. SUBJECT TERMS

Fiber optics
Analog photonics
Photodiodes
Linearization

16. SECURITY CLASSIFICATION OF:			**17. LIMITATION OF ABSTRACT**	**18. NUMBER OF PAGES**	**19a. NAME OF RESPONSIBLE PERSON**
a. REPORT	**b. ABSTRACT**	**c. THIS PAGE**			Meredith N. Hutchinson
Unclassified Unlimited	Unclassified Unlimited	Unclassified Unlimited	Unclassified Unlimited	19	**19b. TELEPHONE NUMBER** *(include area code)* (202) 767-9549

Standard Form 298 (Rev. 8-98)
Prescribed by ANSI Std. Z39.18

CONTENTS

I EXECUTIVE SUMMARY

RF photonic links impress information on modulated optical carriers as a method of transporting high frequency and microwave information over sizeable distances. If the system bandwidth is greater than one octave, the system must contend with the possibility of second order intermodulation distortion (IMD2) creating spurious tones due to nonlinearities. These spurious tones masquerade as signals and impair the performance of the photonic link. Earlier research has shown the utility of defining a nonlinear coefficient that relates the nonlinear second order distortion from two optical tones to the product of the powers of those tones. This nonlinear coefficient was shown to be a function of (i) the bias voltage applied to the photodiode / load resistor combination (V_{tot}), (ii) the DC level of current through the photodiode, I_{DC}, and (iii) the IMD output frequency.

In this work, we propose procedures for minimizing the link impairments due to nonlinearity in the link's photodiode by adaptively biasing the photodiode. In particular, we present two techniques: (i) a method of setting the photodiode bias voltage as a function of the average current through the photodiode, and (ii) a method by which suspicious tones, if not eliminated, can at least be identified as being caused by IMD. This second technique requires an interaction of the system with the input signal, and has two versions. We present schematic illustrations of how the techniques can be implemented.

II INTRODUCTION

The faithful transmission of radio frequency (RF) analog signals is important in applications ranging from wireless backhaul to radar signal processing. Such transport was effected by transmission over coaxial cable in the past, but the advent of semiconductor lasers with improved linearity and stability as well as electro-optic modulators with well-understood transfer functions have made optical transmission over photonic links preferable. In the last several decades, RF photonic links have become the standard approach for transport of high frequency RF information.

In essence, a photonic link interposes an optical transport system between an electronic RF source and its destination. Often, the RF signal is imposed on an optical carrier by modulating its intensity, and the modulated light is transported over an optical fiber to the destination. The low loss, lightweight, linear, interference-free optical medium delivers this optical signal to a receiver which converts the modulated optical signal back to electronic form for further processing.

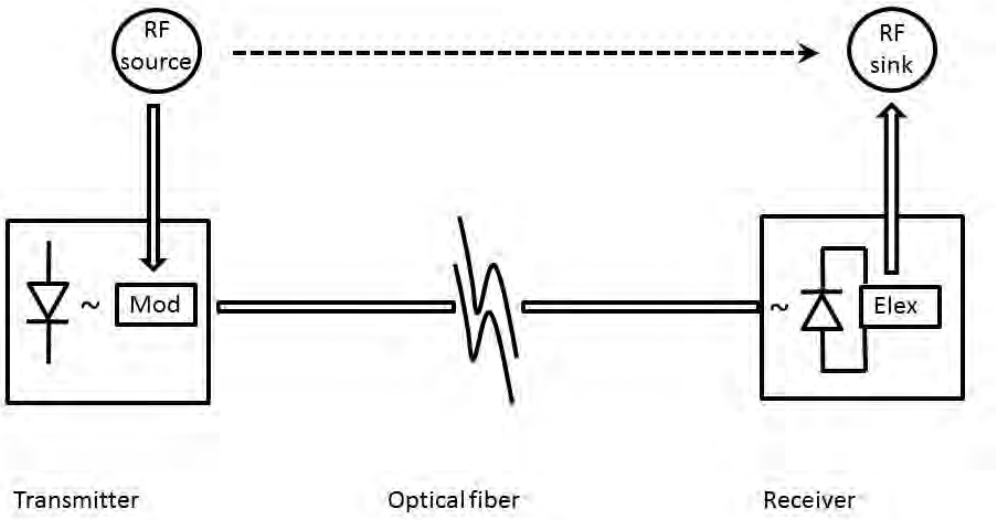

Fig. 1: Basic RF photonic link. RF electrical source modulates light at the transmitter. This light is launched into an optical fiber, and is transported to the receiver. At the receiver, the modulated optical signal is converted back to electrical form by the photodiode, and then delivered to its destination.

RF links, then, have three basic components: the transmitter, optical medium, and the receiver. The transmitter, typically implemented with an electro-optic modulator, has a well known sinusoidal transfer function. As such, third order nonlinearities are dominant, but with proper biasing the second order nonlinearity can be suppressed. In contrast, the fiber is the most robust component: optical nonlinearities are weak and would first show up at optical sum and difference frequencies. That leads to an assessment of the nonlinearity of the photodiode in second order.

Manuscript approved August 11, 2016.

III PHOTODIODE NONLINEARITY

In principle, the photodiode is a linear device. That is, each incident photon has a high probability of creating an electron-hole pair in the absorption region, and these carriers are swept out of the absorption region to be recombined in the external circuit: basically, each absorbed photon creates an external electron in the detector circuit. However, the diode is not perfect, and a standard phenomenological treatment of its nonlinear behavior assumes that its behavior can be modeled as a memoryless transfer function relating the output photocurrent to the input light intensity [1].

Photodiodes are quite efficient and nearly linear, as a practical matter, and to a reasonable approximation the photocurrent is proportional to the incident optical power. In the links we contemplate, the optical intensity I for a single modulated optical carrier with modulation index m would look like

$$I(t) = I_{dc} + I_{ac} = I_{dc} + mI_{dc}\cos\Omega t = I_{dc} + I(\Omega)\cos\Omega t \tag{1}$$

for an incident optical signal. For an ideal photodiode, the resultant electrical current would have the form, to within a constant for the diode responsivity,

$$i(t) = i_{dc} + i_{ac} = i_{dc} + i(\Omega)\cos\Omega t + \ldots . \tag{2}$$

That is, the electrical current would largely mirror the optical intensity and higher order terms can often be ignored. In a real photodiode, especially at its highest frequencies, the responsivity is a function of frequency, with an amplitude and a phase. The determination of this parameter is of great interest to system designers.

In characterizing the nonlinear behavior of the output current, the most obvious method would be to Taylor expand the output current in powers of the input optical intensity. We recently proposed [2, 3] an efficient shortcut which retains the flavor of the expansion, but puts it in a systems context. Our approach is to consider the ideal received photocurrent, i_{ac} as the expansion parameter: it is close to a scaled version of the optical intensity and is readily accessible in experiments. Our motivation was to provide a tool by which quick and automated characterizations could be performed. With this assumption, the output current of the photodiode can be expressed [1] as the expansion

$$i_{out} = i_{dc} + i_{ac} + a_2 i_{ac}^2 + \ldots \tag{3}$$

where we have normalized the ac outputs to the observed ac inputs. For a two-tone input signal, this would result in an expected ac current of

$$i_{ac} = i_1 \sin\omega_1 t + i_2 \sin\omega_2 t\ . \tag{4}$$

That is, if we were to observe the photodiode output on an electrical spectrum analyzer (ESA) we would see components at ω_1 and ω_2. Since the ESA records RF power, we would observe electrical powers of $P_1 \approx i_1^2$ and $P_2 \approx i_2^2$ at the two frequencies, where we ignore the scale factors due to the input coupling and photodiode responsivity.

To calculate the second order mixing tones, we substitute Eqn. (4) into Eqn. (3), and expect an output current of

$$\begin{aligned} i_{out} \approx i_1 \sin\omega_1 t + i_2 \sin\omega_2 t + \\ a_2 i_1 i_2 \cos(\omega_1 - \omega_2)t - a_2 i_1 i_2 \cos(\omega_1 + \omega_2)t. \end{aligned} \tag{5}$$

In the presence of a second order nonlinearity, then, we expect power at $|\omega_1 \pm \omega_2|$, the sum and difference RF frequencies. We further assumed [2, 3] that the magnitude of the nonlinear coefficient a_2 was a function of the output frequency. Then, since

$$P(|\omega_1 \pm \omega_2|) \propto a_2(|\omega_1 \pm \omega_2|)^2 i_1^2 i_2^2\ ,$$

we can scale powers to $P_0 \equiv 1\ mW$, making conversion to dBm more convenient, and use the standard $R = 50\ \Omega$ termination to arrive at a dimensionless measure of the nonlinearity defined as [3]

$$\gamma_2(|\omega_1 \pm \omega_2|)_{dB} \equiv 10\ log_{10}\left[\frac{2P_0}{R}a_2^2(|\omega_1 \pm \omega_2|)\right] = P(|\omega_1 \pm \omega_2|)_{dBm} - P(\omega_1)_{dBm} - P(\omega_2)_{dBm}. \quad (6)$$

In this form, γ_2 can be determined directly from reading the ESA powers at $\omega_1,\ \omega_2,\ |\omega_1 - \omega_2|$, and $\omega_1 + \omega_2$. As observed earlier [3], this characterization can be automated and it provides a map of the second order nonlinearity of a photodiode as a function of the output IMD frequency, parameterized on the operation point.

IV MEASURING SECOND ORDER DISTORTION IN PHOTODIODES

A slightly modified version of an experimental setup described earlier [2, 3] was used to evaluate γ_2 and is shown below. Two independent laser sources are modulated with Mach-Zehnder modulators held

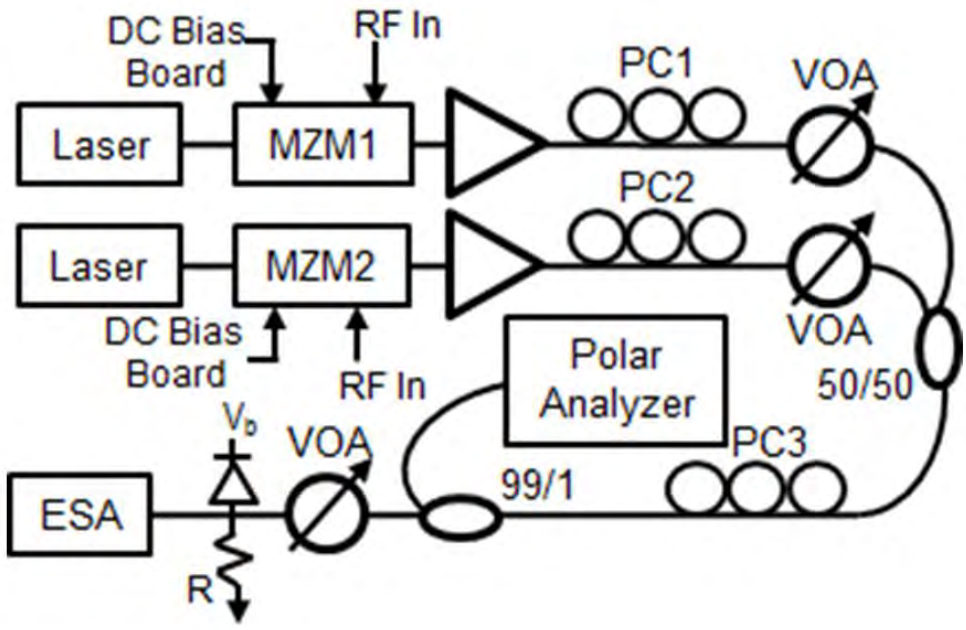

Fig. 2: Experimental setup (See Refs. [2, 3]). Two laser sources are independently modulated with quadrature-stabilized Mach-Zehnder modulators (MZM), combined in a 50/50 coupler, sent to a photodiode, and analyzed by an electrical spectrum analyzer (ESA). Polarization controllers allowed independent as well as collective polarization conditions to be analyzed by a polarimeter (Polar Analyzer). A variable optical attenuator was placed before the photodiode to permit changes in the photocurrent.

at quadrature with bias boards, and the light from each is combined and sent to the photodiode under test. Polarization rotators permitted the states of polarization to be changed independently or together. Another

optical attenuator was placed before the photodiode to permit controlled attenuation of the photocurrent without disturbing the remainder of the experimental setup. An electrical spectrum analyzer (ESA) observed the RF powers at both fundamentals as well as the sum and difference frequencies. Data was recorded from the ESA, corrected for cable loss, then sorted and plotted as a function of output frequency for a large number of (V_b, I_{dc}) operation points.

An example of the output data for one operation point [2, 3] is shown in Fig. 3 . In this figure, nonlinear

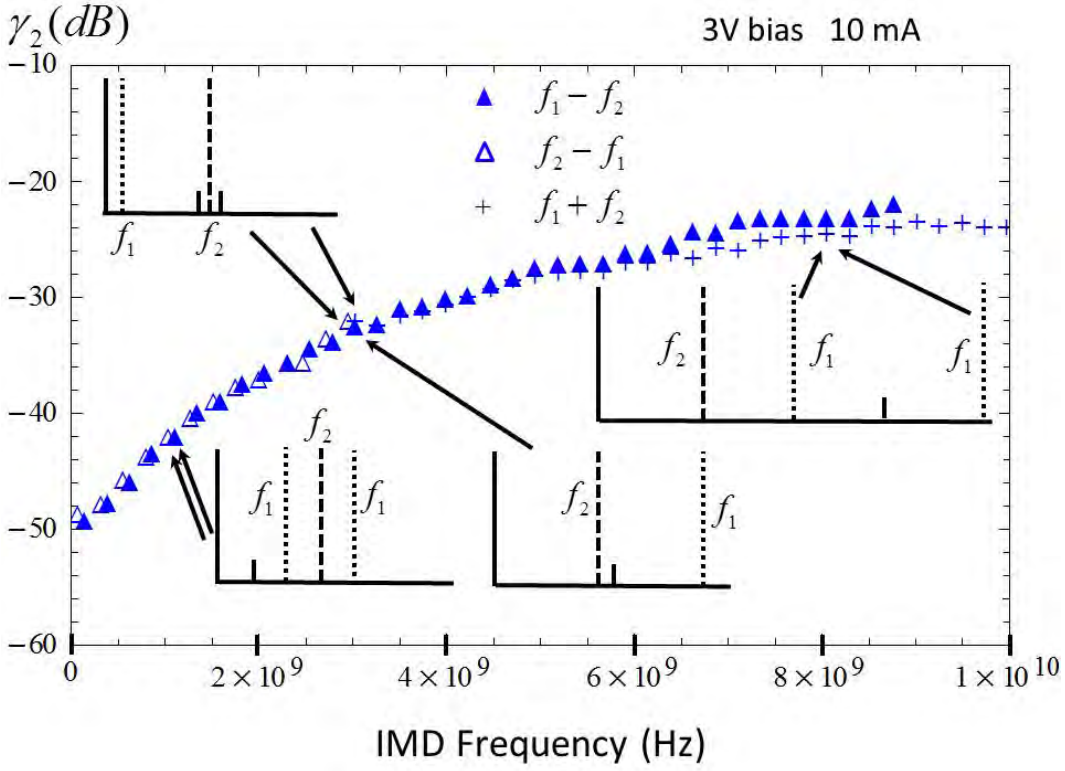

Fig. 3: Typical experimental trace. Operation point was ($V_b = 3\ V,\ I_{dc} = \ 10\ mA$). Modulation frequency f_1 was swept while f_2 was held constant at 3 GHz. All three types of IMD products are shown: "low difference" tones ($f_1 < f_2$) and "high difference" tones ($f_1 > f_2$) are shown as empty and filled triangles, respectively, while sum tones are shown with a "+" symbol. Despite the different frequency plans for the IMD products, the nonlinear coefficient γ_2 falls on a single curve when the products are sorted by output frequency. (From Ref. [3])

products for all three types of frequency plans (i.e., difference frequencies when $f_1 < f_2$ and $f_1 > f_2$, as well as sum frequencies) are plotted $vs.$ their IMD frequency for the operation point with bias voltage $V_b = 3\,V$ and average current $I_{dc} = 10\,mA$. It is clear that the value of γ_2 tends to follow a general curve. While other shapes of curves are observed as well as the "well behaved" curve in Fig. 3, it is clear that such plots can be used to construct an objective function or figure of merit for a photodiode's nonlinear performance. For instance, one might specify the greatest value of γ_2 over the test range, or perhaps the greatest value of γ_2 over the range $2\ GHz < f_{IMD} < 6\ GHz$ as a specification for a system design. By surveying a large set of (V_b, I_{dc}) operation points, one could then construct a performance surface over the feasible range for a given system. Such a surface would permit, for example, a system to be set at an

operation point that minimizes the nonlinear distortion.

V SYSTEM VIEWPOINT

We completed a survey on one of our photodiodes, a commercial p-i-n diode with a $10\ GHz$ bandwidth. For an array of operation points, curves such as that in Fig. 3 were taken. For specificity, we used as an objective function the maximum value for γ_2 over the entire range of IMD frequencies up to $10\ GHz$. A set of experiments were run, over a set of bias voltages ($2\ V \leq V_b \leq 8\ V$) and average currents ($2\ mA \leq I_{dc} \leq 12\ mA$), with the results shown in Fig. 4. For each (V_b, I_{dc}) operation point, a curve such

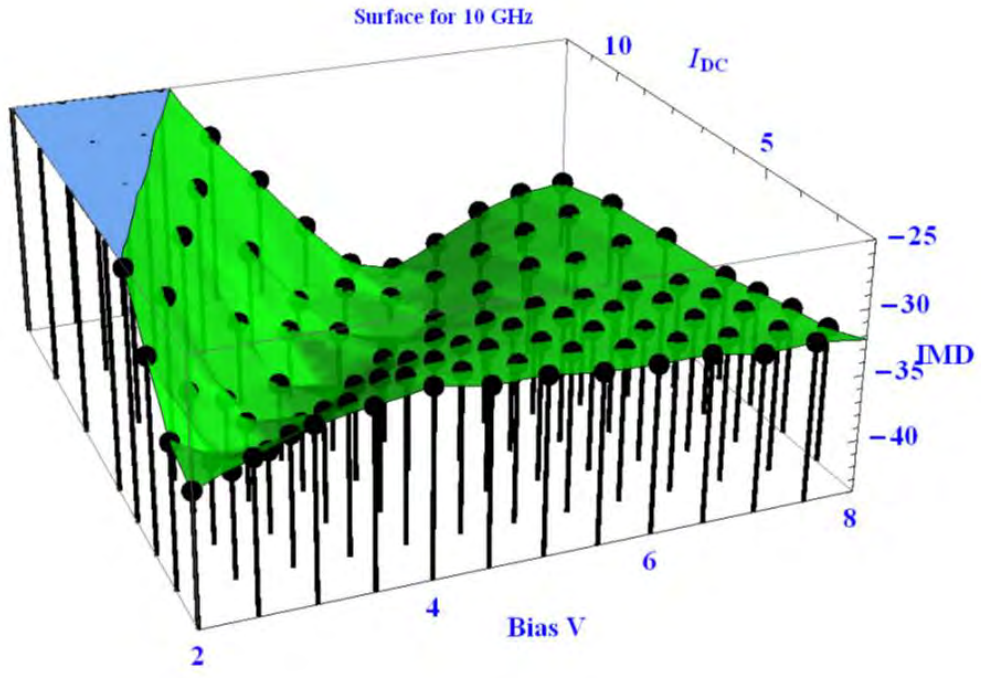

Fig. 4: Surface of nonlinear coefficients for photodiode. Each vertical stick represents a (V_b, I_{dc}) operation point: a curve such as that in Fig. 3 is taken, and the maximum value of γ_2 for that curve is plotted as a heavy dot at the top of the stick representing that curve. A numerical interpolation function is fit through data points, and is plotted.

as that in Fig. 3 was taken. The maximum value of γ_2 over the $10\,GHz$ range was recorded. At the (V_b, I_{dc}) co-ordinates for that operation point, a heavy dot is plotted on the third axis at a position corresponding to the maximum γ_2 observed. To aid the eye, a vertical line is drawn upward to terminate at that heavy point. Given this array of points in 3D, a third order interpolation function was fit through the observed data and is plotted as a green surface. If the interpolated fit were perfect, each heavy dot would have half its volume above the surface. One can see that this surface has some structure: there is a "valley" running from the lower left point ($2\ V,\ 2\ mA$) to about the midpoint ($6\ V,\ 12\ mA$) of the top boundary.

The surface in Fig. 4 is an approximation to a system specification for the minimal second order IMD

for this photodiode. That is, since it represents the worst case performance for IMD2 at each operation point, it could be taken as a specification for nonlinearity performance. As such, optimal operation points would be those points located at the lowest points on the surface. Another view is given in Fig. 5: the data is the

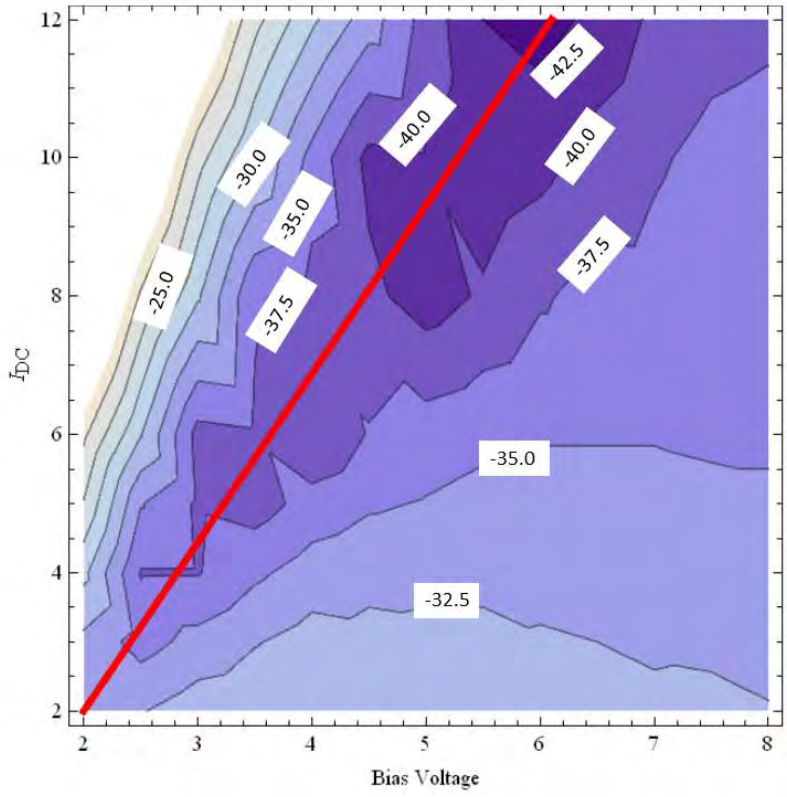

Fig. 5: Contour plot of the experimental values for maximum γ_2. At each (V_b, I_{dc}) operation point, a curve as in Fig. 3 is taken and the maximum value for γ_2 over the entire $10\,GHz$ range is determined. An interpolating function for the set of data points in Fig. 4 is calculated, and the contours are determined numerically. The labeled levels on contours are the maximal values for γ_2 in dB for this numerical function. A line with a slope of $1/250\Omega$ approximates the set of feasible optimal operation points.

same as in Fig. 4, but is read as a contour plot of the interpolated surface function, and reveals the "valley" of Fig. 4 in a quantitative way. Again, this data should be viewed as a system specification: for instance, at the operation point $(5\,V, 9\,mA)$, Fig. 5 indicates that, over the $10\,GHz$ range, one expects, at worst, $\gamma_2 \approx -40\,dB$. In light of the variation in γ_2 shown in operation point plots (for instance, Fig. 3 shows a variation of $\approx 25\,dB$), the nonlinear performance at most IMD frequencies might be much better than this level, but the point of a specification is to identify the worst or limiting performance of a component or subsystem.

The fact that there is structure in the contour plot holds open the possibility that system performance might be optimized to exploit the characteristics of a given photodiode. That is, one would prefer, *ceteris paribus*, to operate at a point as low as possible on the surface. In this vein, we point out the red line in Fig. 5: it is roughly coincident with the set of optimal operation points, and corresponds to the equation

$$I_{dc} = 2mA + \frac{V_b - 2V}{400\,\Omega}. \tag{7}$$

Guiding a system to its optimal operation point is the purpose of this memo, and the subject to which we now turn.

VI ADAPTIVE BIASING

Introduction

The preceding section illustrated that, from a systems perspective, the nonlinearity penalty for operating a system can be optimized by choosing the operation point. Imagine a link as in Fig. 1 operating at an optimal point, such as $(3\,V, 4\,mA)$. This point is optimal in the following sense. The photodiode is at the end of the link and the optical intensity of the incoming signal is a parameter that it can't control: the transmitter's launch power and the link losses are variables outside of the control of the receiver. Roughly speaking, a high efficiency photodiode will create approximately one carrier pair for each photon absorbed, so the carrier generation rate (and hence the average current) is approximately set by the optical power at the receiver. The only other parameter the receiver can adjust is the bias voltage V_b. Assume there are two RF tones on the optical carrier(s) that each develop RF powers $P_i = -40\,dBm$ signals at their respective frequencies. The IMD2 signals developed will depend on the frequencies of the two tones, as Fig. 3 suggests. But from a system perspective, the worst case can be found, from either Fig. 4 or Fig. 5: these show that $\gamma_2 \leq -37.5\,dB$, which translates into an IMD2 power of $-117.5\,dBm$ by virtue of Eqn. 6. On the other hand, if the receiver were biased at $5\,V$, for instance, Fig. 5 and Eqn. 6 indicate an additional performance penalty on the order of $4.5\,dB$, since γ_2 increases by that amount in making such a change in bias voltage. This penalty flows directly onto the spurious-free dynamic range (SFDR) for this impairment. Illustratively, for a noise floor of approximately $-122\,dBm$, the IMD2 signal is buried in the noise for the optimal bias of $3\,V$, but is $4.5\,dB$ above the noise floor for a $5\,V$ bias. In other words, this IMD2 signal would present a ghost signal and would degrade the system's SFDR. We are thus led to the notion that the nonlinearity performance of a system can be affected, and thus optimized, by changing the operation point.

The basic idea of this notion, which we call "adaptive biasing," is simple: utilize knowledge of the photodiode properties to adjust the bias of a photodiode in such a way that the penalties from nonlinear intermodulation products are mitigated. There are several approaches we propose here that can implement this goal.

Bias setting from current detection

The first approach is exploit the map we have already discussed above in Fig. 5, in which the photodiode has been characterized and an approximate set of optimal operation points are known. We can illustrate this operation by considering the operation of a link as shown below in Fig. 6. As before, assume the system is optimally biased at $(3\,V, 4\,mA)$, represented by state A. Now suppose that, for whatever reason, the system power increases by $3\,dB$: this results in a new average photocurrent of $8\,mA$, and a new state, represented by B on Fig. 6. At point B, the maximum γ_2 has increased by approximately $10\,dB$ to $-27.5dB$. This increased nonlinearity leads to IMD2 powers increasing by $10\,dB$ by virtue of Eqn. 6. These larger spurious signals are a direct degradation of the system performance by $10\,dB$. (Note that we are talking about a *system* specification: there are *some* frequency plans for which this impairment is realized, but any individual frequency plan may or may not reflect this penalty. But since the system specification is the "worst performance over all frequencies" in our assumed case, the system metric has decreased by this amount.) At this point, however, the system has recognized the increased current. Assuming that a feedback loop of some sort (e.g. a voltage source driven by a current mirror or a digitally controlled bias voltage) has implemented Eqn. 7, the bias voltage would increase to $4.4\,V$, driving the system to operating point C. At this operation

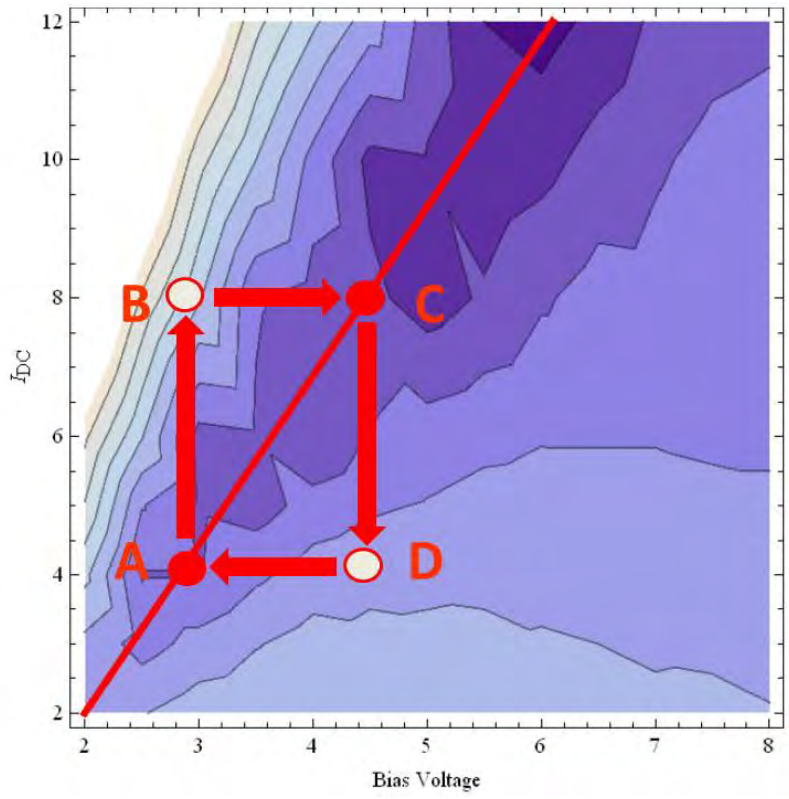

Fig. 6: Illustration of adaptive biasing by current sensing (see text). System is initially operating in optimal operation point A. Input power increases by $3\,dB$ to $8\,mA$, moving the system to operation point B, with a $10\,dB$ reduction in SFDR. The system senses the increased current, and adjusts the bias voltage to bring the system to a near optimal operation point, C. The process is similar for a reduction in power, taking the system from C $\rightarrow$ D $\rightarrow$ A.

point, $\gamma_2 \approx -39\,dB$, and the improvement, relative to operation point B is approximately $11.5\,dB$, and the SFDR specification improves by the same amount. Note that now, at point C, the system's performance is *also* better (by about $1.5\,dB$) than it was at point A. However, that performance improvement was *not* available at point A: at that point, the system was optimally biased. This points out that the optimality is necessarily local (as determined by I_{dc}), since the receiver does not (at least in this simplified system) have the option of changing the average current.

If the system, operating at point C, were now to experience a reduction in power such that the average current returned to $4\,mA$, it would now find itself at point D in Fig. 6. The nonlinearity specification at this point is approximately $-33.5\,dB$, which is not optimal biasing for this current. Discovering that it was off the optimal line described by Eqn. (7), the system would adjust the bias to $V_b = 3\,V$, returning to the original point for an improvement in the SFDR specification of about $4\,dB$.

A functional schematic of an implementation of this idea is shown in Fig. 7. A voltage proportional to the photocurrent in photodiode (PD) is choked or low-pass filtered and its dc level is detected (Level), providing an estimate for I_{dc}, the vertical coordinate for the operation point on Figs. 5 and 6. This voltage level is then conditioned (Cond) and sent to a series-pass regulator to set the bias voltage, i.e., the horizontal coordinate for the operation point. The implementation can be achieved in a variety of ways, such as analog

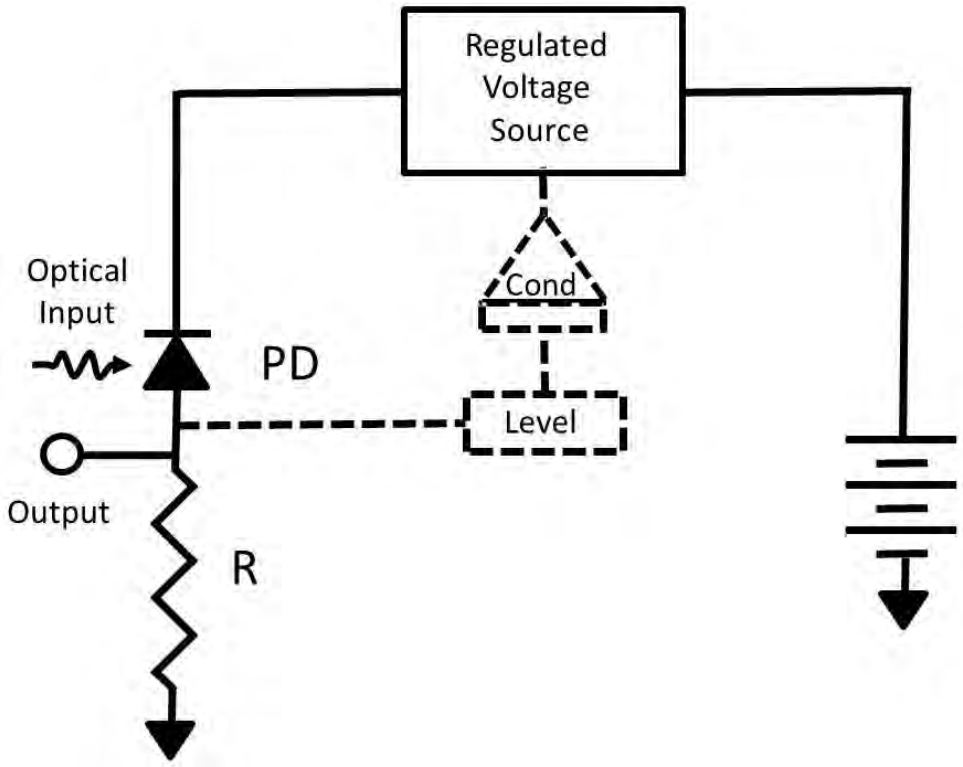

Fig. 7: Implementation of current detection. Average dc level of current through photodiode (PD) is detected (Level) and conditioned (Cond) to set the bias voltage through a series-pass voltage regulation circuit. The circuitry in dashed outline is designed to mimic the optimal line for operation points as in Figs. 5 and 6.

techniques using current mirror circuits or digital techniques in which the sensed level is analyzed and creates the input to a digital-to-analog converter. Although analog techniques are conceptually simpler, we envision that the low bandwidth needed (probably on the order of kHz) to follow variations in average current through the PD, as well as flexibility in handling startup and transient conditions, would make digital implementations more cost effective and robust.

We mention in passing that this section has assumed that only the bias voltage can be controlled. In principle, it should also be possible to regulate the optical power by installing an optical preamplifier with a programmable optical attenuator in front of the photodiode. In this case, the system has that second degree of freedom to adjust, so a global minimum can be achieved. Such an implementation would add optical noise to the circuit, and its usefulness would be determined by the various noise floors. This degree of freedom could also be used in implementations discussed in the next section. However, in the spirit of simple realizations of the ideas we propose here, we only mention this as a possibility and will not describe it further.

Ghost detection through interactive analysis of output spectrum

Introduction

Generally speaking, the impairment caused by photodiode nonlinearities can be viewed as the creation of "ghost tones" in the output spectrum, as if viewed on a spectrum analyzer. Imagine, for instance, a system in which a wide RF spectrum is being surveyed and displayed on an ESA. Various system noise sources create a "noise floor" at the bottom of the display which plots RF spectral intensity $vs.$ RF frequency. Above the noise floor, we can envision spikes corresponding to tones at various frequencies and strengths. Given large spikes at, say $5\,GHz$ and $6\,GHz$, and a much smaller spike at $1\,GHz$, the issue is the identification of that $1\,GHz$ tone: is it a real source, or is it a "ghost," an intermodulation product caused by the two stronger tones at 5 and $6\,GHz$? This, in essence, is the SFDR measure for the system.

In this section, we describe another adaptive biasing technique which can help the operator extend the system's utility. If we assume that the real information needed by the operator is the knowledge of whether or not a spectral feature is a ghost or not. If it were not a ghost, we could extend the effective system SFDR by helping the operator identify the feature as a ghost. In that case, the presence of the tone is merely an annoyance and not a limit.

This proposal involves an interaction of the detection system with the signals it detects. That is, if a tone is suspected to be a ghost tone, the system will change its characteristics and re-evaluate the tone after the change. It requires that the candidate tone be persistent over enough time for the system to identify the tone and devise a reaction: it will not work if the candidate tone appears and then disappears instantly. Assuming this, we envision a situation in which a small candidate tone appears on the spectrum and persists for multiple spectral scans. The central idea is that by changing the bias voltage, one might be able to observe characteristics in the candidate tone's perceived power that would enable the operator to identify it as a ghost tone.

Photodiode response

We first establish that the photodiode's response is somewhat insensitive to the bias voltage. Intuitively, this can be understood as the fact that the photodiode efficiently harvests electron-hole pairs created by absorbed photons.[1] For a given incident optical signal, the carrier pairs created are either fruitfully collected into the external circuit and observed, or may diffuse internally and recombine before making it to the external circuit. One expects that an increase in the bias voltage would help sweep the carriers more efficiently into the external circuit, and this is qualitatively borne out in Fig. 8. An experiment was performed on the setup shown in Fig. 2. RF tones $f_1 = 1.4\,GHz$ and $f_2 = 1.9\,GHz$ were impressed on the two $MZMs$ corresponding to two different optical powers: at the ESA, the detected tones had nominal RF powers of $P_1 = -30\,dBm$ and $P_2 = -68\,dBm$ at the detector. The RF powers were recorded for bias voltages ranging from $1\,V$ to $8\,V$, inclusive, in steps of $1\,V$. Since $I_{dc} = 10\,mA$, this forms a set of 8 points near the top of Figs. 5 and 6. To make a grid on these figures, we also decreased I_{dc} in steps of $2\,mA$ by attenuating the optical signal on the PD with the final VOA in Fig. 2. In addition to attenuating the dc current, however, this also attenuated the ac signal by the same ratio. To facilitate comparison, we normalized all observed RF powers by adding an attenuation correction of $20\,log_{10}(I_{dc}/10\,mA)\;dB$ to the observed power. At the same time, we observed the powers in the lower power tone at f_2. Again, to facilitate comparison, we applied the same attenuation correction as for f_1, and also added $37.9\,dBm$ to compensate for the lower power of f_2. For an ideal photodiode, all 80 experiments (two tones, 8 bias levels, 5 attenuation levels) would fall on a horizontal line. In fact, there are three non-idealities: (i) There is an uncertainty in each measurement,

[1] In this and further discussions, we also incorporate the idea that there may be an increased likelihood of impact ionization or other nonlinearities.

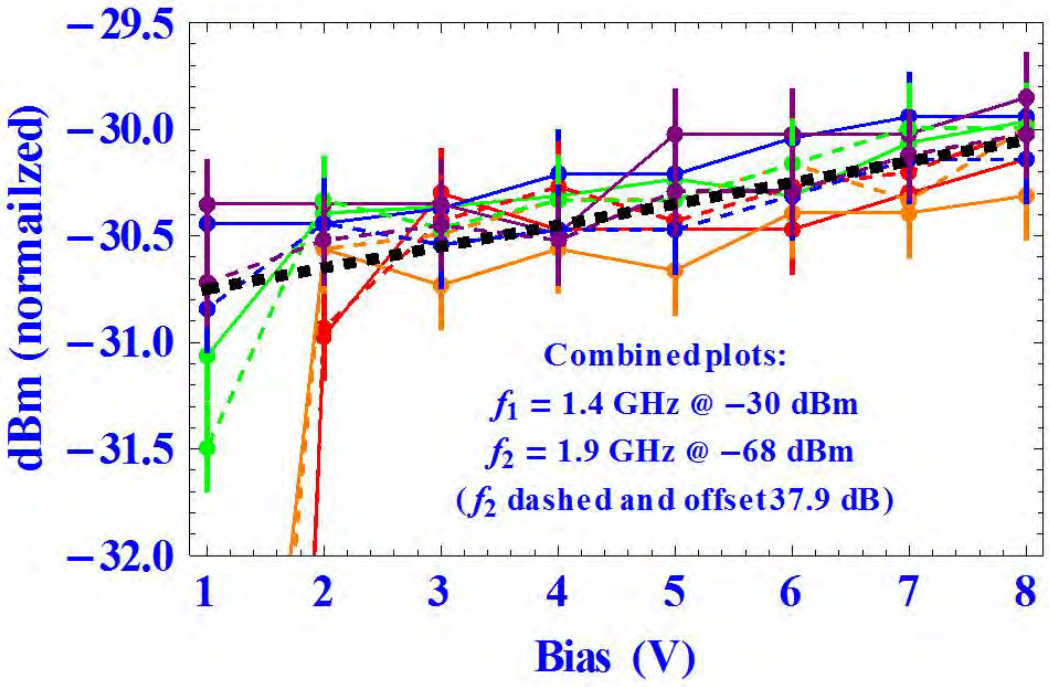

Fig. 8: Variation in photodiode gain for RF modulated tones $vs.$ bias voltage. Observed ESA power at two frequencies for a range of bias voltages. Each curve represents a different I_{dc}, which was obtained by optical attenuation: average currents of $(10, 8, 6, 4, 2)\,mA$ are represented by (red, orange, green, blue, purple) curves, respectively. Nominal RF powers for $10\,mA$ operation was $-30\,dBm$ for tone at $1.4\,GHz$ (solid colors) and $-68\,dBm$ for tone at $1.9\,GHz$ (dashed colors). For comparison, the RF powers were scaled for variations in current, and the lower power tones were shifted by $37.9\,dBm$. A black dashed curve with slope $0.1\,dB/V$ is drawn in to guide the eye.

shown as error bars, (ii) There is a general upward trend with increasing bias voltage, and (iii) there is a marked fall off below $2\,V$ bias. This last point is understandable: above a few mA current, the diode is saturated at the lowest bias voltages[3] and the heavy carrier production can not be efficiently swept out of the photodiode's absorption region. Point (i) is an inherent limitation on accuracy in the instrumentation: our estimate of $0.2\,dB$ errors corresponds to an accuracy of about 5%: further increases in accuracy would require extraordinary measures. When operating in a non-saturated condition, point (ii) indicates that increasing bias voltage increases the efficiency with which each carrier pair is harvested in the external circuit: greater voltages would be expected to increase the drift (vs. diffusion) component of the carrier motion, and thus increase the external current[4]. As an aid to the eye, a line with a slope of approximately $0.1\,dB/V$ is overlaid on the plot. This behavior is quite sub-linear: $0.1\,dB$ corresponds to a 2.3% in output power (which corresponds to half that percentage change in photocurrent), while $1\,V$ bias change corresponds to between 14% and 50% changes in bias voltage at the high and low bias points, respectively.

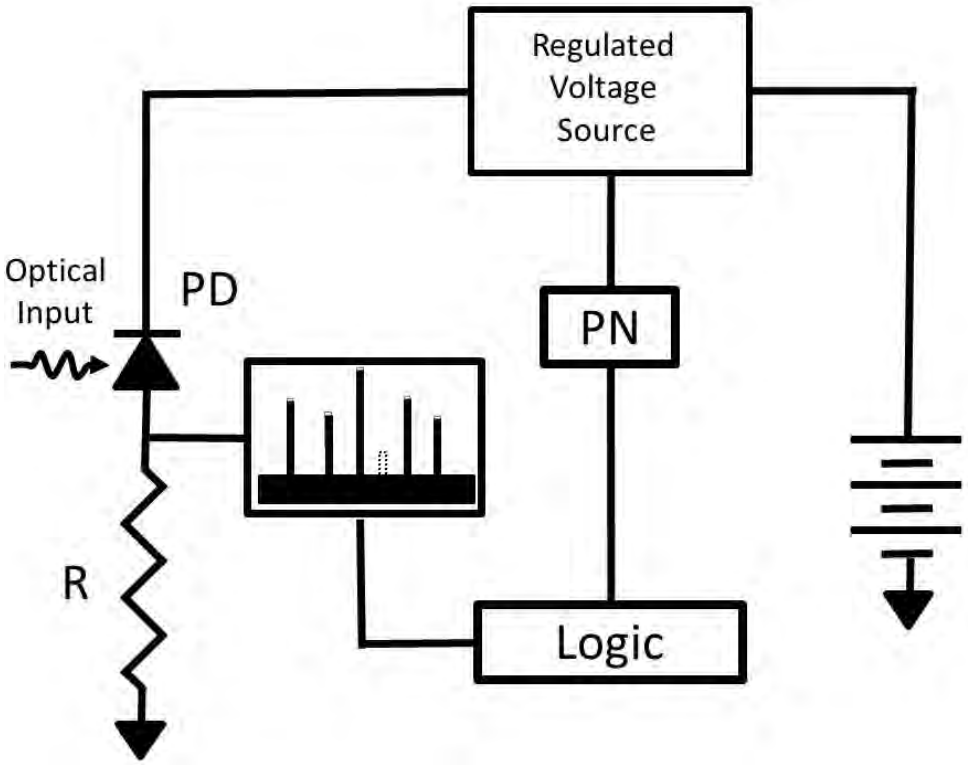

Fig. 9: Schematic of technique to identify ghost tones. RF spectrum of input is analyzed by a processor (Logic) and candidate tones are identified as possible ghost tones (faint tone, 4th from left in display). Processor directs a signal, illustratively a pseudo-noise generator (PN), to change the bias voltage in a series of steps. This causes real tones to vary slightly, but the ghost tones to vary much more significantly in power, "winking" in step with the PN sequence (4th from left in display). Such tones are certainly ghosts.

Implementing ghost identification

In short, a change in detected output power is very weakly connected to changes in the bias voltage. We can exploit this fact to identify ghost traces, and the basic scheme is illustrated in Fig. 9. A system is shown, in which the PD output is illustratively displayed on an ESA, a proxy for the system's detection apparatus. A candidate tone (4th from left on display in Fig. 9) has appeared: is it a ghost or real target? A logic circuit identifies the fact that this candidate tone is questionable, and signals a dithering signal, illustratively a pseudonoise generator (PN), to create an identifiable code. The string is sent to a voltage regulator that controls the bias voltage on the photodiode. For real signals, the PN code will have a minimal and predictable effect on the displayed power, as can be gleaned from Fig. 8. Each real tone's displayed power would change by roughly $0.1\,dB/V$ in lock step with the PN sequence. However, if the candidate is a ghost tone, it is expected to behave differently. First, since it is a product, its displayed power will change by twice the amount that the real tones change, by virtue of Eqn. 6. More important, however, is the much wider variation exhibited by the change in the nonlinear coefficient γ_2 when the operation point is changed. An indication of this is given in Figs. 5 and 6. Those contours are the values for the maximum γ_2, but since all of the γ_2 curves tend toward higher values at the top end of the RF spectrum, these contours minimize the variations seen at individual frequencies: it is common to see variations of $20\,dB$ for bias changes of

$1\,V$. Consequently, as the PN sequence is run, the real tones will have minimal changes while the ghost tones will "wink" on and off with possibly very large variations in displayed power. These variations can be autocorrelated with the known PN sequence to enhance the probability of ghost detection.

In summary, the technique laid out in this section offers a method by which changes in bias will not eliminate the ghost tones: they will still exist on the system display. However, they offer the expectation that these ghost tones can be identified as such, so that functionally the utility of the detection system has increased: the SFDR has been increased in application even though spurious tones appear on the passive display. It is important to note that pathological cases could occur: if the PN code amplitude is fixed, it is possible that the winking will be minimal due to an accidental odd combination of frequency plans and nonlinear behavior. This technique's test for ghosts delivers no false positives but can deliver a false negative. That is, a ghost tone can masquerade as a real tone, but a real tone won't masquerade as a ghost tone.[2]

Coupling device characteristics and signal tones

Our final proposal is, in a sense, an extreme version of the preceding section: it requires detailed understanding of the photodiode characteristics and the signal spectrum. It would be implemented physically in much the same way as in Fig. 7, but the demands on the logic block would be much more substantial. In this case, the PN codes would be running continuously, but the detailed curves similar to Fig. 3 would be stored and available for reference. Several implementations would be possible. For instance, one might set a threshold to look at the highest power tones, create a table of candidate IMD tones, use the technique of the previous section to look at the outputs (i.e. the responses to the PN modulation of the bias voltage) and, if the particular products of the tones at this frequency plan and operation point are ambiguous, add or subtract a constant voltage to the PN code to move to another operating point. This needn't be done in real time: there could be an evolving data stream, say the top 100 peaks as (frequency, power) pairs that could be accessed. The processing and discrimination could then be thought of as a background cleanup utility that scrubs the files to eliminate signals that can be traced to spurious IMD.

A similar approach that uses the same characterization information, can be used to drive the system to the exact operation point needed to minimize any one of a set of mixing tones (from an analysis of a set of stored curves similar to Fig. 3) that could create a spurious tone at a candidate frequency. The desire to implement such a process, costly in processing power, would depend on an ability to either pipeline the analysis on a separate processor or a compelling need to identify specific distortion sources.

Techniques such as these are clearly more costly in processing power, but offer the ultimate in system performance: by identifying and filtering out spurious data, the effective SFDR of the system could be enhanced tremendously. That is, rather than accepting the "passive" estimation[3] of a system's SFDR, one could use a detailed knowledge of the photodiode properties to essentially eliminate nonlinearity as a system impairment and push to more fundamental limits to system performance.

VII SUMMARY

We have presented a set of approaches to reduce the system impairments caused by photodiode second order IMD in photonic links. We reviewed earlier work which showed that the nonlinear properties of photodiodes can be characterized as a function of the (bias voltage, average current) operation point, and

[2]This is reminiscent of a quote by Damon Runyon: "The race is not always to the swift, nor victory to the strong, but that's the way you bet."

[3]By this we mean optimization in the "mini-max" sense of Section VI: one accepts the minimum value for the maximum IMD products over the system range.

showed that there are optimal biasing points at each value of the administered variable[4] which can be reached by controlling the bias voltage. We proposed several approaches, which we term "adaptive biasing" to exploit the existence of these optimal points. In one approach, we sense the average current through the photodiode and use that information to set the bias to the operation point that minimizes the maximum impairment over all frequency plans the system might see. This impairment, as a "mini-max" solution, is fairly simple to implement but generally does not yield the minimal achievable impairment for *all* display frequencies. It can be viewed as extending the SFDR and assuring a system specification. In addition to this "passive" approach, which is independent of the incident signals, we also presented versions in which the system reacts to a set of signals, changes its characteristics, observes the effects these changes have on the set of signals, and then evaluates the likelihood that members of the signal set are spurious or "ghost" tones. These approaches require that signals are persistent enough in time that the system can react and evaluate, and require more processing power than the passive approach. We presented two versions of this approach: in one, the operation point was modulated and the effect on the signal was indeterminate, and in the other, the operation points were selected to do precise discrimination of candidate tones. The first was "blind" and allowed false negatives (ghost tones could possibly masquerade as real), while the other was more computationally intensive but promised to effectively eliminate second order distortion.

[4] In other words, we consider the average photocurrent (admittedly a coordinate of the operation point) to be set by the incident power on the photodiode and thus not under the receiver subsystem's control.

VIII REFERENCES

[1] Urick, V.J., McKinney, J.D., and Williams, K.J. *Fundamentals of Microwave Photonics*, Wiley, Hoboken, NJ, 2015.

[2] M.N. Hutchinson, N.J. Frigo, and J.R. Peasant, "Novel characterization and analysis of photodiode intermodulation distortion, paper SM3R.8, CLEO 2016, San Jose, CA, 5 - 10 June 2016 .

[3] N.J. Frigo, M.N. Hutchinson, and J.R. Peasant, "Characterization of photodiode nonlinearities by output frequency analysis," submitted to *J. Lightwave Tech.* Special Issue on Microwave Photonics 2016.

[4] K.J. Williams, R.D. Esman, and M. Dagenais, "Nonlinearities in p-i-n microwave photodetectors," *J. Lightwave Tech.*, vol. 14(1), pp. 84 - 96 (1996).